Development of large area hexagonal boron nitride quasi-bulk crystals

J. Y. Lin[a)] and H. X. Jiang[a)]

Department of Electrical and Computer Engineering, Texas Tech University, Lubbock, TX 79409, USA

ABSTRACT

Ultrawide bandgap (UWBG) semiconductors have the potential for superior performance and are poised to make a huge impact in electronic and photonic devices. In the III-nitride family, the crystal growth and use of hexagonal BN (*h*-BN) with a bandgap around 6 eV, remain relatively underdeveloped. Drawing parallels to GaN technology, advancing crystal growth techniques to produce thick epitaxial films or quasi-bulk crystals in larger wafer sizes with high crystalline quality is essential for propelling *h*-BN as a viable material for UWBG electronic and photonic devices. In this overview, we summarize recent advancements in synthesizing large-diameter wafers of *h*-BN quasi-bulk crystals, achieved through hydride vapor phase epitaxy (HVPE), resulting in epitaxial layers exceeding hundreds of microns (100s' μm) in thickness. Notably, our group has attained high-efficiency direct conversion neutron detectors, demonstrating a record detection efficiency of 60% for thermal neutrons and 2.2% for fast neutrons. These significant developments represent a crucial steppingstone toward further enhancing crystal growth technologies to produce electronic-grade *h*-BN. This material has the potential to serve as both an active host and substrate for diverse applications, including photonics, power electronics, neutron detection, and quantum information technology.

Keywords: Ultrawide bandgap (UWBG) semiconductors, hexagonal BN, epitaxial growth, quasi-bulk crystal growth, solid-state neutron detectors

1. INTRODUCTION

It is well recognized that the performance metrics of semiconductor electronic devices are intricately linked to the material's energy bandgap (Eg) in a highly non-linear fashion. III-nitride wide bandgap semiconductor light-emitting diodes (LEDs) and power electronic devices have revolutionized the energy sector by providing brighter, more energy-efficient, and reliable lighting solutions as well as power conversion systems [1-9]. These innovations have significantly lowered energy consumption and reduce environmental impacts. Our invention of III-nitride microLED technology made over two decades ago [10-13] has given rise to the microLED display industry, spurring research into microLED microdisplays for applications in augmented reality, virtual reality, and three-dimensional (AR/VR/3D) displays [10-14].

While high In-content InGaN and Al-content AlGaN alloy-based photonic devices are advancing the capabilities of full-spectrum solar energy [15-17], sterilization, and UV curing technologies [18,19], the application of hexagonal boron nitride (*h*-BN) as an ultrawide bandgap (UWBG) semiconductor is still significantly underexplored. This is despite *h*-BN's remarkable physical properties, which include an UWBG of around 6 eV at room temperature [20-24], a high breakdown field of 13 MV/cm [25,26], and impressive in-plane thermal conductivity of about 550 W/m·K [27]. Much of the existing research on *h*-BN has concentrated on monolayers or few-layer

Quantum Sensing and Nano Electronics and Photonics XXI, edited by Manijeh Razeghi, Giti A. Khodaparast, Miriam S. Vitiello, Proc. of SPIE Vol. 13376, 133760A
 · 0277-786X · doi: 10.1117/12.3040091

structures for the construction of 2D based heterostructures [28] and for optically stable single photon emitters [29], typically produced through exfoliation techniques that depend on millimeter-sized bulk crystals grown using high-pressure, high-temperature (HPHT) methods [21, 24-26] and metal flux solution approaches [23,27]. However, these methods face significant challenges when scaling larger wafer and device sizes.

Notably, *h*-BN is exceptionally well-suited to produce direct conversion solid-state neutron detectors [30-38]. This distinctive capability is largely due to the presence of boron-10 (B-10), one of the few isotopes that have a favorable nuclear capture cross-section for thermal neutrons, measuring 3840 barns [39, 40]. As a result, the absorption length for thermal neutrons in B-10 enriched *h*-BN (*h*-^{10}BN) is 47 μm, while it reaches 237 μm in natural *h*-BN [30-39]. These substantial absorption lengths underscore the urgent need for the development of large-area, thick *h*-BN epitaxial films or quasi-bulk wafers. We present a brief overview of recent advancements in the production of large-diameter *h*-BN quasi-bulk wafers with thicknesses in the hundreds of micrometers, utilizing hydride vapor phase epitaxy (HVPE), a well-established growth technique for growing GaN and AlN quasi-bulk crystals with high growth rates reaching 100s of μm per hour [41, 42]. The first active devices that require the use of *h*-BN quasi-bulk crystals that we have successfully demonstrated include thermal neutron detectors with a record high efficiency and fast neutron detectors with practical efficiency, the results of which will be discussed.

2. EXPERIMENT, RESULTS AND DISCUSSIONS

The HVPE growth processes for producing high quality *h*-BN possess similar challenges as for AlN [41, 42], which also require the abilities to support high growth temperatures typically above 1300 ^{0}C and mitigate the issue of parasitic reactions in the gas phase. To grow *h*-BN wafers, BCl_3 and NH_3 gases were used as precursors [43-46]. The growth was conducted on c-plane sapphire. At a growth temperature of 1450 ^{0}C, the growth rate was about 15 μm/h. As illustrated in Fig. 1(a), *h*-BN has a layered crystalline structure and a close lattice-match to graphite and hence to graphene, with the spacing between the stacked layers in the c-direction of 3.33 Å, giving a c-lattice constant of c=6.66 Å. Due to its layered crystalline structure, *h*-BN self-separates from sapphire to form a freestanding and flexible wafer during cooling process after growth [33-38, 43-46]. This self-separation phenomenon offers several benefits, including easier wafer dicing, reusing sapphire substrates, and fabrication of devices in flexible forms (e.g., in stacked or curved configurations).

In Figure 1(b), a cross-sectional view of transmission electron microscope (TEM) image is shown for a freestanding *h*-BN quasi-bulk wafer of 100 μm in thickness produced by HVPE by authors' group [39], which directly reveals that the spacing between the stacked planes in the c-direction to be 3.33 Å. Figures 1(c) plots a Raman spectrum of a freestanding *h*-BN quasi-bulk wafer [39]. The observed mode at $\Delta\sigma$ = 1366 cm^{-1} is related to the E_{2g} vibration mode (in-plane stretch of B and N atoms) and corresponds well with the expected Raman peak of bulk *h*-BN [39], suggesting that these freestanding HVPE wafers are strain free. Figures 1(d) shows XRD pattern in $2\theta - \omega$ scan of the sample in a large angle range, revealing the *h*-BN (002) peak position (diffraction from stacked planes in the c-axis direction) centered at $2\,\theta$ = 26.72° [45], corresponding to a c-lattice constant of nearly 6.66 Å, corroborating the TEM measurements results shown in Fig. 1(b). Diffraction peaks from *h*-BN (002), (004), and (006) planes (stacked planes in the c-axis direction) were clearly observable, which indicates that these *h*-BN quasi-bulk crystals have a very good long-range order in the direction of c-axis.

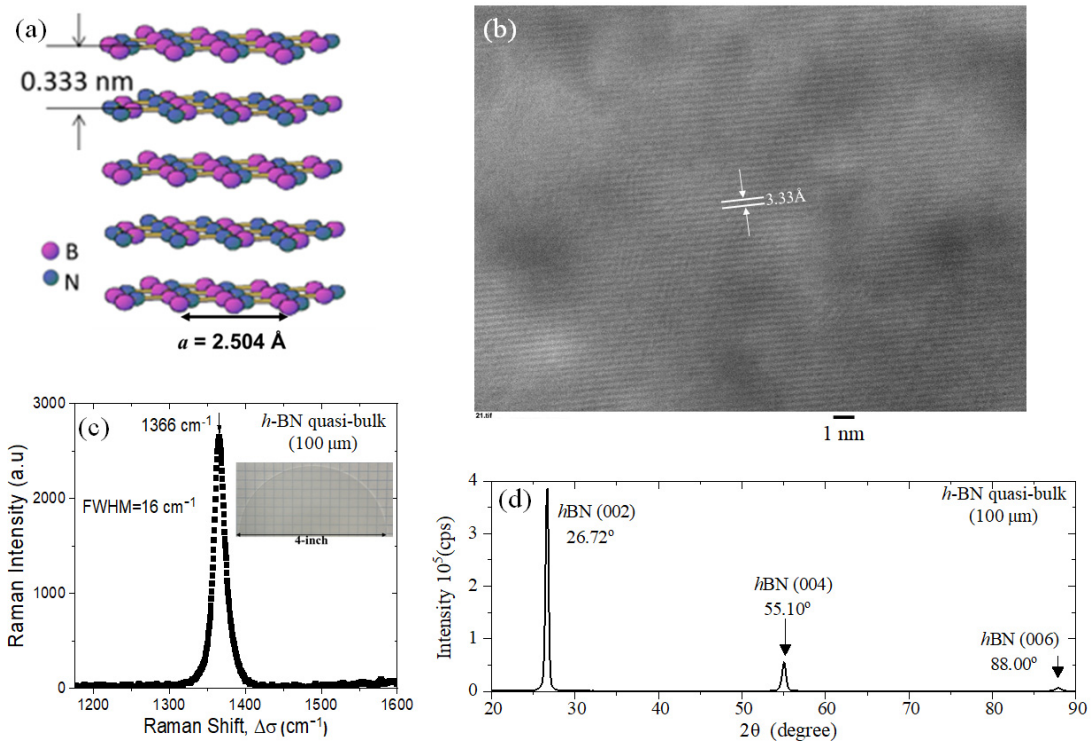

Figure 1. (a) Schematic of crystalline structure of *h*-BN showing a c-lattice constant of c=6.66 Å and spacing between stacked layers in the c-axis direction of 3.33 Å. (b) Cross-sectional view of TEM image of a 100 μm thick freestanding *h*-BN quasi-bulk wafer produced by HVPE, measuring a spacing of 3.33 Å between the stacked layers in the c-axis direction. (c) Room temperature Raman spectrum of a 100 μm thick *h*-BN quasi-bulk wafer produced by HVPE. The inset shows a photo of a 4"-diameter freestanding *h*-BN quasi-bulk wafer. (a)-(c) Figures reproduced from Ref. 39 under the terms of the Creative Commons Attribution 4.0 license, N. K. Hossain, A. Tingsuwatit, Z. Alemoush, M. Almohammad, J. Li, J. Y. Lin, and H. X. Jiang, "Probing room temperature indirect and minimum direct band gaps of *h*-BN," Appl. Phys. Express **17**, 091001 (2024). (d) XRD pattern obtained in a 2θ-ω scan in a large angle range. Figure reproduced from Ref. 45 under the terms of the Creative Commons CC BY license, Z. Alemoush, A. Tingsuwatit, A. Maity, J. Li, J. Y. Lin and H. X. Jiang, "Status of *h*-BN quasi-bulk crystals and high efficiency neutron detectors," J. Appl. Phys. **135**, 175704 (2024).

The TEM, XRD and Raman results shown in Fig. 1 all indicate that HVPE grown quasi-bulk crystals have a pure *h*-phase (layered structure). Since the Raman mode shown in Fig. 1(c) results from the in-plane stretch of B and N atoms, its FWHM directly correlates with the structural ordering in the c-plane. The observed FWHM of the E_{2g} vibration mode in h-BN quasi-bulk wafers of 16 cm^{-1} is broader than those in samples grown by HTHP of typically 8-10 cm^{-1} [46].

A high efficiency *h*-BN thermal neuron detector must have a large layer thickness to ensure a sufficient thermal neutron absorption (high intrinsic efficiency), following $\eta_i = 1 - e^{-d/\lambda}$, where λ (*h*-^{10}BN) = 47 μm and λ (*h*-BN) = 237 μm. Moreover, to ensure an effective collection of the radiation-generated charge carriers by the electrodes, the recombination or capture lifetime (τ) of radiation-generated charge carriers must exceed the transit time (τ_t), meaning $\tau \geq \tau_t$. The transit time of the charge carriers can be expressed as the transit distance divided by the velocity (μE) of the charge carriers. Thus, the charge collection condition can also be written as $\mu\tau E >> W$, or equivalently $\frac{\mu\tau V}{W^2} >> 1$, where *E* (*V*) denotes the applied electric field (bias voltage) and *W* is the width (thickness) of a *h*-BN lateral (vertical) device. Electrical transport characterization results

indicated that the $\mu\tau$ products in the c-plane are about 2 orders of magnitude larger than those align the c-axis [35, 47, 48]. As such, we have developed lateral detector architecture by taking advantage of *h*-BN's superior lateral transport properties [35-38, 45]. The typical lateral $\mu\tau$ products of these quasi-bulk materials are in the order of 1 x 10^{-4} cm^2/V [43]. This means that the detector's width should be designed to be smaller than 4 mm, W < 4 mm, for an operating voltage of 450 V. As shown schematically in the inset (1) of Fig. 2(a), by connecting multiple narrow lateral detectors in parallel, large area detectors can be constructed. Each narrow detector strip within the large detector has metal contacts covering the entire vertical edges of the detector of 100 μm in thickness to ensure that the electric field is uniformly applied in the c-plane through the bulk of the h-BN detector. An optical image of a finished 1 cm^2 area detector fabricated by combining 6 detector lateral strips fabricated from a *h*-^{10}BN quasi-bulk wafer (100 μm thick) is shown in the inset (2) of Fig. 2(a).

A Californium-252 (^{252}Cf) source in conjunction with a cube made of hig*h*-density polyethylene (HDPE) moderate was to serve as a thermal neutron source [31-37]. The thermal neutron detection efficiencies were measured by placing the detectors at 30 cm from the HDPE block front face and side by side with a ^{6}LiF filled micro-structured semiconductor neutron detector (MSND) with a known detection area (4 cm^2) and detection efficiency (30%). By measuring the counts against that of the MSND detector, the detection efficiencies of *h*-^{10}BN detectors can be obtained. The sensitivity of *h*-^{10}BN to gamma photons was tested by measuring the pulsed height spectra (PHS) of *h*-^{10}BN detector in the presence of a 662 keV ^{137}Cs source and the results indicated that the sensitivity of *h*-^{10}BN detectors to gamma photons from 662 keV ^{137}Cs source is at the background level [31, 36, 45]. This is because BN is composed of low atomic elements B and N.

Figure 2(a) plots the measured detector efficiency (η) as a function of the applied voltage (and electric field) [45], which shows that at a bias voltage of 450 V, this 1 cm^2 area detector delivers a record high detection efficiency for thermal neutrons of 60%. By defining the charge collection efficiency (η_C) as the ratio of the measured efficiency to theoretical efficiency of $\eta_i = 1 - e^{-d/\lambda}$, Fig. 2(a) also plots η_c as a function of the applied voltage, yielding a maximum collection efficiency of 68%. The value of η_c is also a good measure of *h*-BN material quality, and the ideal value of η_c is 100%.

On the other hand, the interaction cross-section between fast neutrons (neutrons with energies > 1 MeV) and matter is extremely low. To detect fast neutrons with energy larger than 1 MeV, the process of elastic scattering of fast neutrons with detector's constituent elements is utilized, which typically has a cross-section in the order of ~ 2 Barn [49-51]. Consequently, the detection of fast neutrons is regarded technically challenging. The measured mean free paths in *h*-BN for neutrons emitted from bare ^{252}Cf and AmBe neutron sources are 7.6 cm and 5.2 cm, respectively [38, 53]. This means that detectors with a thickness d > 7.6 cm (or 5.2 cm) are needed to achieve *h*-BN fast neutron detectors with an intrinsic detection efficiency exceeding 63% (=1-e^{-1}) for fast neutrons with a comparable average energy as those emitted from ^{252}Cf (or AmBe) source.

Recently, we have successfully produced 0.4 mm thick freestanding *h*-BN 4"-diameter wafers [52]. The 400 μm thick freestanding wafer was subjected to mecahnical polish to thin down to about 350 μm in thickness to improve the surface smoothness and then cut into strips of 1.3 mm in width and 7.5 mm in length via laser dicing. By stacking 4 such layers together, a total thickness of 1.4 mm was achieved. A schametic illustration of a 4-layer vertical stacked *h*-BN detectors is shown in inset (1) of Fig. 2(b). The optical image of a finished 4-layer vertical stacked *h*-BN fast

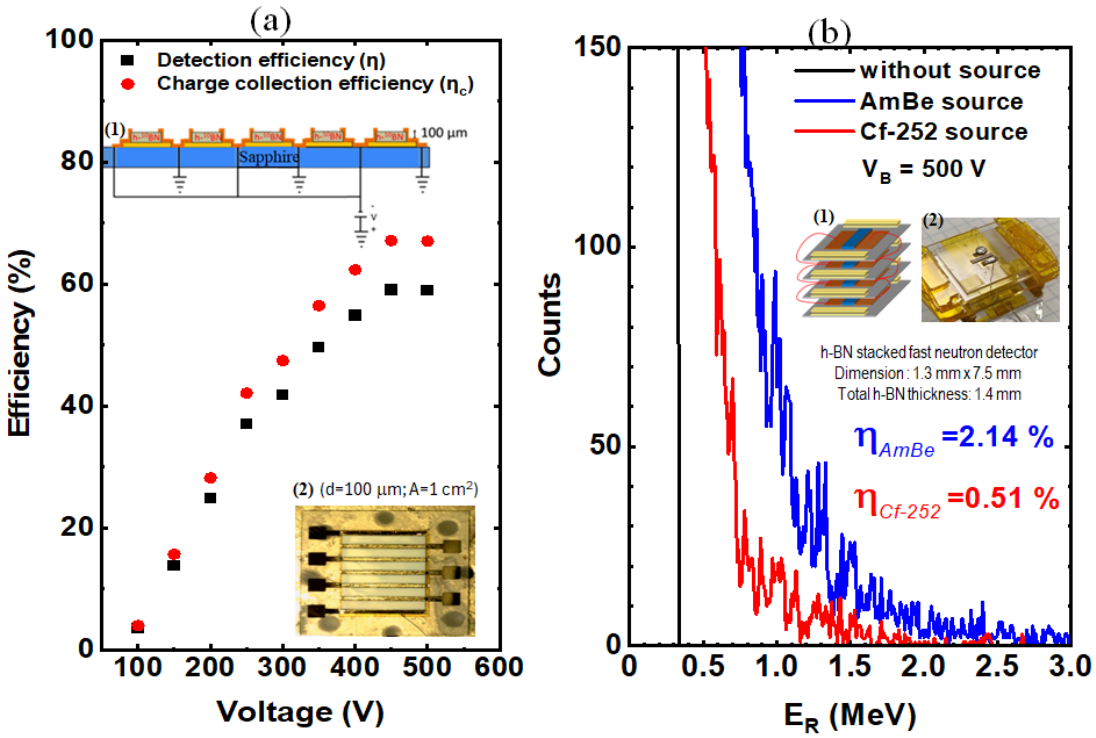

Figure 2. (a) Plot of measured detection efficiency (η) and effective charge collection efficiency (η_c) as functions of the applied voltage of a 1 cm^2 area *h*-BN thermal neutron detector fabricated from a 100 μm thick *h*-^{10}BN wafer. Inset (1) Schematic illustration of a multi-strip detector constructed by connecting multiple narrow detector strips in parallel to form a large area detector. Inset (2) Optical image of a finished 1 cm^2 area thermal neutron detector formed by connecting in parallel 6 detector strips fabricated from a 100 μm thick *h*-^{10}BN wafer. Figures reproduced from Ref. 45 under the terms of the Creative Commons CC BY license, Z. Alemoush, A. Tingsuwatit, A. Maity, J. Li, J. Y. Lin and H. X. Jiang, "Status of *h*-BN quasi-bulk crystals and high efficiency neutron detectors," J. Appl. Phys. **135**, 175704 (2024). (b) Pulsed height spectra (PHS) acquired by a 1.4 mm thick *h*-BN fast neutron detector (constructed by staking four 350 μm thick detectors) in response to fast neutrons from bare ^{252}Cf source (red curve) and AmBe source (blue curves) without the use of a HDPE moderator and in absence of any source (black curve), all measured at a bias voltage V_B=500 V with detector located at 10 cm from the sources. A pyrolytic BN (p-BN) film of 2.1 mm in thickness is used to block any thermal neutrons from these two neutron sources. Schematic illustration of forming a thick detector by stacking multiple layered detectors is shown in inset (1). Optical image of a finished 1.4 mm thick fast neutron detector is depicted in inset (2). Figures reproduced from Ref. 52 under the terms of the Creative Commons CC BY license, J. Li, A. Tingsuwatit, Z. Alemoush, J. Y. Lin, and H. X. Jiang, "Ultrawide bandgap semiconductor *h*-BN for direct detection of fast neutrons," APL Materials **13**, 011101 (2025).

neutron detector is shown in inset (2) of Fig. 2(b). For AmBe source, the measured detection efficiency of this 1.4 mm thick detector is 2.2% [52], corresponding to a charge collection efficiency of 81% calculated by using the intrinsic efficiency value of 2.7% based on a mean free path of 5.2 cm in *h*-BN for fast neutrons from AmBe source. For ^{252}Cf source, the measurement results yielded a detection efficiency of 0.51% [52]. To the best of our knowledge, this is the first demonstration of a semiconductor detector that can detect fast neutrons directly with a measured efficiency of more than 2%.

Detectors that are capable of sensing both thermal and fast neutrons have many important applications in critical and emerging areas of technologies, including nuclear and fusion reactors

power and safety monitoring, nuclear security, nuclear waste management, oil field exploration, neutron imaging and therapy, fundamental research in nuclear and particle, plasma and materials sciences, and life search beyond earth.

3. SUMMARY

We presented a concise overview of the current status of *h*-BN quasi-bulk wafer development. Structural characterization results indicate that *h*-BN quasi-bulk wafers, with a thickness of 100 μm, exhibit a favorable stacking sequence and long-range order along the c-axis. Thermal neutron detectors with a detection area of 1 cm^2, designed in a lateral geometry from 100 μm thick boron-10 enriched *h*-BN wafers, have achieved a record thermal neutron detection efficiency of 60% at a bias voltage of 450 V. Furthermore, direct detection of fast neutrons using *h*-BN UWBG semiconductor detectors has been successfully demonstrated, with a detection efficiency of up to 2.2% achieved by a stacked detector with a total thickness of 1.4 mm in response to neutrons emitted from a bare AmBe neutron source. *h*-BN is increasingly recognized as an important UWBG material for various applications, including deep ultraviolet (UV) photonics, substrates for two-dimensional devices, hyperbolic dispersion devices with innovative uses, single-photon emitters, and qubits. These applications stand to benefit significantly from the availability of high-quality, large-diameter quasi-bulk wafers. Consequently, the development of large-diameter *h*-BN quasi-bulk materials is vital to serve as active medium or substrate for these advanced technologies.

ACKNOWLEDGEMENT

The efforts of *h*-BN quasi-bulk crystal growth and high efficiency neutron detector developments were funded in part by the Advanced Research Projects Agency-Energy (ARPA-E), U.S. Department of Energy, grant Nos. DE-AR0001552, DE-AR0001257, DE-AR000964, and DE-AR0001821, monitored by Dr. Olga Spahn, Dr. Isik Kizilyalli, and Dr. Eric Carlson. The views and opinions of authors expressed herein do not necessarily state or reflect those of the United States Government or any agency thereof. The authors are grateful to the AT&T Foundation for the support of Ed Whitacre and Linda Whitacre endowed chairs.

REFERENCES

a) jingyu.lin@ttu.edu; hx.jiang@ttu.edu

1. S. Pimputkar, J. S. Speck, S. P. DenBaars, and S. Nakamura, "Prospects for LED lighting," Nature Photon 3, 180 (2009).
2. H. Amano, N. Sawaki, I. Akasaki, and Y. Toyoda, "Metalorganic vapor phase epitaxial growth of a high quality GaN film using an AlN buffer layer," Appl. Phys. Lett. ***48****, 353 (1986).*
3. S. Nakamura, T. Mukai, and M. Senoh, "Candela-class hig*h*-brightness InGaN/AlGaN double-heterostructure blue-light-emitting diodes," Appl. Phys. Lett. **64**, 1687 (1994).
4. M. A. Khan, R. A. Skogman, R. G. Schulze, and M. Gershenzon, "Electrical properties and ion implantation of epitaxial GaN, grown by low pressure metalorganic chemical vapor deposition," Appl. Phys. Lett. **42,** 430 (1983).
5. M. Asif Khan, A. Bhattarai, J.N. Kuznia, and D.T. Olson, "High electron mobility transistor based on GaN-AlxGa1-xN heterojunction," Appl. Phys. Lett. **63**, 1214 (1993).

6. H. Amano, Y Baines, E Beam *et al*., "The 2018 GaN power electronics roadmap," J. Phys. D: Appl. Phys. **51** 163001 (2018).
7. I. C. Kizilyalli, O. B. Spahn, and E. P. Carlson, "Recent progress in wide-bandgap semiconductor devices for a more electric future," ECS Trans. **109**, 3 (2022).
8. Y. H. Chen, J. Encomendero, C. Savant, V. Protasenko, H. G. Xing, and D. Jena, "Electron mobility enhancement by electric field engineering of AlN/GaN/AlN quantum-well HEMTs on single-crystal AlN substrates," Appl. Phys. Lett. **124**, 152111 (2024).
9. J. Y. Tsao, S. Chowdhury, M. A. Hollis, D. Jena, et al., "Ultrawide-Bandgap Semiconductors: Research Opportunities and Challenges," Adv. Electron. Mater. **4**, 1600501 (2018).
10. S. X. Jin, J. Li, J. Z. Li, J. Y. Lin and H. X. Jiang, "GaN microdisk light emitting diodes," Appl. Phys. Lett. **76**, 631 (2000).
11. H. X. Jiang, S. X. Jin, J. Li, J. Shakya, and J. Y. Lin, "III-nitride blue microdisplays," Appl. Phys. Lett. **78**, 1303 (2001).
12. J. Day, J. Li, D. Y. C. Lie, Charles Bradford, J. Y. Lin, and H. X. Jiang, "III-Nitride full-scale high-resolution microdisplays," Appl. Phys. Lett. **99**, 031116 (2011).
13. H. X. Jiang and J. Y. Lin, "How we made the microLED," Nat Electron **6**, 257 (2023).
14. P. J. Parbrook, B. Corbett, J. Han, T. Y. Seong, and H. Amano, "Micro-Light Emitting Diode: From Chips to Applications," Laser Photonics Rev. **15**, 2000133 (2021).
15. J. Wu, W. Walukiewicz, K. Yu, J. W. Ager III, E. E. Haller, H. Lu, W. J. Schaff, Y. Saito, Y. Nanishi, "Small band gap bowing in InGaN alloys," Appl. Phys. Lett. **80**, 4741 (2002).
16. S. Vanka, B. Zhou, R. A. Awni, Z. Song, F. A. Chowdhury, X. Liu, H. Hajibabaei, W. Shi, Y. Xiao, I. A. Navid, A. Pandey, R. Chen, G. A. Botton, T. W. Hamann, D. Wang, Y. Yan, and Z. Mi, "InGaN/Si Double-Junction Photocathode for Unassisted Solar Water Splitting," ACS Energy Lett. **5**, 3741(2020).
17. Y. Zhao, M. Xu, Xuanqi H. J. Lebeau, T. Li, D. Wang, H. Fu, K. Fu, X. Wang, J. Y. Lin, and H. X. Jiang, "Toward High Efficiency at High Temperatures: Recent Progress and Prospects on InGaN-Based Solar Cells," Materials Today Energy, **31**, 101229, (2023).
18. M. A. Khan, K. Balakrishnan and T. Katona, "Ultraviolet light-emitting diodes based on group three nitrides," Nature Photon **2**, 77 (2008).
19. Z. Zhang, M. Kushimoto, T. Sakai, N. Sugiyama, L. J. Schowalter, C. Sasaoka, and H. Amano, "A 271.8 nm deep-ultraviolet laser diode for room temperature operation," Appl. Phys. Express **12**, 124003 (2019).
20. T. Sugino, K. Tanioka, S. Kawasaki, and J. Shirafuji, "Characterization and Field Emission of Sulfur-Doped Boron Nitride Synthesized by Plasma-Assisted Chemical Vapor Deposition," Jpn. J. Appl. Phys., Part **2** 36, L463 (1997).
21. K. Watanabe, T. Taniguchi, and H. Kanda, "Direct-bandgap properties and evidence for ultraviolet lasing of hexagonal boron nitride single crystal," Nat. Materials **3**, 404(2004).
22. B. Arnaud, S. Lebe`gue, P. Rabiller, and M. Alouani, "Huge Excitonic Effects in Layered Hexagonal Boron Nitride," Phys. Rev. Lett. **96**, 026402 (2006).
23. Y. Kubota, K. Watanabe, O. Tsuda, and T. Taniguchi, "Deep ultraviolet light-emitting hexagonal boron nitride synthesized at atmospheric pressure," Science **317**, 932 (2007).
24. G. Cassabois, P. Valvin and B. Gil, "Hexagonal boron nitride is an indirect bandgap semiconductor," Nature Photonics **10**, 262 (2016).

25. Y. Hattori, T. Taniguchi, K. Watanabe, and K. Nagashio, “Anisotropic dielectric breakdown strength of single crystal hexagonal boron nitride,” ACS Appl. Mater. Interfaces **8**, 27877 (2016).
26. Y. Hattori, T. Taniguchi, K. Watanabe, and K. Nagashio, “Comparison of device structures for the dielectric breakdown measurement of hexagonal boron nitride” Appl. Phys. Lett. **109** 253111 (2016).
27. C. Yuan, J. Li, L. Lindsay, D. Cherns, J. W. Pomeroy, S. Liu, J. H. Edgar and M. Kuball, “Modulating the thermal conductivity in hexagonal boron nitride via controlled boron isotope concentration,” Communications Physics **2**, 43 (2019).
28. A. K. Geim and I. V. Grigorieva, “Van der Waals heterostructures,” Nature **499**, 419 (2013).
29. R. Bourrellier, S. Meuret, A. Tararan, O. Stephan, M. Kociak, L. H. G. Tizei, and A. Zobelli, “Bright UV single photon emission at point defects in *h*-BN,” Nano Lett. **16**, 4317 (2016).
30. J. Li, R. Dahal, S. Majety, J.Y. Lin, and H.X. Jiang, "Hexagonal boron nitride epitaxial layers as neutron detector materials," Nuclear Inst. and Methods in Physics Research Section A **654,** 417 (2011).
31. T. C. Doan, S. Majety, S. Grenadier, J. Li, J. Y. Lin, and H. X. Jiang, “Fabrication and characterization of solid-state thermal neutron detectors based on hexagonal boron nitride epilayers,” Nuclear Inst. and Methods in Physics Research Section A **748**, 84 (2014).
32. K. Ahmed, R. Dahal, A. Weltz, J.-Q. Lu, Y. Danon and I. B. Bhat, “Growth of hexagonal boron nitride on (111) Si for deep UV photonics and thermal neutron detection,” Appl. Phys. Lett. **109**, 113501 (2016).
33. A. Maity, T. C. Doan, J. Li, J. Y. Lin, and H. X. Jiang, “Realization of highly efficient hexagonal boron nitride neutron detectors,” Appl. Phys. Lett. **109**, 072101 (2016).
34. A. Maity, S. J. Grenadier, J. Li, J. Y. Lin, and H. X. Jiang, “Toward achieving flexible and high sensitivity hexagonal boron nitride neutron detectors,” Appl. Phys. Lett. **111**, 033507 (2017).
35. A. Maity, S. J. Grenadier, J. Li, J. Y. Lin, and H. X. Jiang, “High sensitivity hexagonal boron nitride lateral neutron detectors,” Appl. Phys. Lett. **114**, 222102 (2019).
36. A. Maity, S. J. Grenadier, J. Li, J. Y. Lin, and H. X. Jiang, “High efficiency hexagonal boron nitride neutron detectors with 1 cm^2 detection areas,” Appl. Phys. Lett. **116**, 142102 (2020).
37. A. Maity, S. J. Grenadier, J. Li, J. Y. Lin, and H. X. Jiang, “Hexagonal boron nitride: Epitaxial growth and device applications,” Prog. Quantum. Electron. **76** 100302 (2021).
38. A. Tingsuwatit, A. Maity, S. J. Grenadier, J. Li, J. Y. Lin, and H. X. Jiang, “Boron nitride neutron detector with the ability for detecting both thermal and fast neutron,” Appl. Phys. Lett. **120**, 232103 (2022).
39. N. K. Hossain, A. Tingsuwatit, Z. Alemoush, M. Almohammad, J. Li, J. Y. Lin, and H. X. Jiang, “Probing room temperature indirect and minimum direct band gaps of *h*-BN,” Applied Physics Express **17**, 091001 (2024).
40. O. Osberghaus, “Die Isotopenhäufigkeit des Bors. Massenspektrometrische Untersuchung der Elektronenstoßprodukte von BF_3 und BCl_3,” Zeitschrift fuer Physik **128** 366 (1950).
41. Y. Kumagai, T. Yamane, and A. Koukitu, “Growth of thick AlN layers by hydride vapor-phase epitaxy Journal of Crystal Growth,” **281**, 62 (2005).
42. Y. Kumagai, K. Goto, T. Nagashima, R. Yamamoto, M. Bockowski. and J. Kotani, “Influence of growth rate on homoepitaxial growth of AlN at 1450 °C by hydride vapor phase epitaxy,” Appl. Phys. Express **15**, 115501 (2022).

43. Z. Alemoush, N. K. Hossain, A. Tingsuwatit, M. Almohammad, J. Li, J. Y. Lin, and H. X. Jiang, "Toward achieving cost-effective hexagonal BN semi-bulk crystals and BN neutron detectors via halide vapor phase epitaxy," Appl. Phys. Lett. **122**, 012105 (2023).
44. Z. Alemoush, A. Tingsuwatit, J. Li, J. Y. Lin, and H. X. Jiang, "Probing boron vacancy complexes in *h*-BN semi-bulk crystals synthesized by hydride vapor phase epitaxy," Crystals **13**, 1319 *(2023)*.
45. Z. Alemoush, A. Tingsuwatit, A. Maity, J. Li, J. Y. Lin and H. X. Jiang, "Status of *h*-BN quasi-bulk crystals and high efficiency neutron detectors," J. Appl. Phys. **135**, 175704 (2024).
46. Y. Li, V. Garnier, P. Steyer, C. Journet, and B. Toury, "Millimeter-scale hexagonal boron nitride single crystals for nanosheet generation," ACS Applied Nano Materials **3**, 1508 (2020**).**
47. S. J. Grenadier, A. Maity, J. Li, J. Y. Lin, and H. X. Jiang, "Origin and roles of oxygen impurities in hexagonal boron nitride epilayers," Appl. Phys. Lett. **112**, 162103 (2018).
48. S. J. Grenadier, A. Maity, J. Li, J. Y. Lin, and H. X. Jiang, "Lateral charge carrier transport properties of B-10 enriched hexagonal BN thick epilayers," Appl. Phys. Lett. **115**, 072108 (2019).
49. G. F. Knoll, Radiation detection and measurement, 4th edition, John Wiley & Sons, (2010).
50. J. R. Dunning, G. B. Pegram, G. A. Fink, and D. P. Mitchell, "Interaction of neutrons with matter," Phys. Rev. **48**, 265 (1935).
51. T. Jevremovic, *Nuclear Principles in Engineering*, 2nd ed., Springer Science+Business Media, LLC 2009.
52. J. Li, A. Tingsuwatit, Z. Alemoush, J. Y. Lin, and H. X. Jiang, "Ultrawide bandgap semiconductor *h*-BN for direct detection of fast neutrons," APL Materials **13**, 011101 (2025).